Resistance anomalies in superconducting mesoscopic Al structures

C. Strunk,* V. Bruyndoncx, C. Van Haesendonck, V. V. Moshchalkov, and Y. Bruynseraede
Laboratorium voor Vaste-Stoffysica en Magnetisme, Katholieke Universiteit Leuven, Celestijnenlaan 200 D, B-3001 Leuven, Belgium

C.-J. Chien, B. Burk, and V. Chandrasekhar
Department of Physics and Astronomy, Northwestern University, 2145 Sheridan Road, Evanston, Illinois 60208

(Received 20 June 1997)

We present a detailed study of the recently reported resistance peaks close to the superconducting transition of quasi-one-dimensional mesoscopic Al structures. It is found that the anomalies can be induced by radio-frequency irradiation or by applying sufficiently high dc currents. The nonmonotonic resistance curves are correlated with excess voltages in the voltage-current characteristics close to the critical current and depend strongly on the temperature and the magnetic field. The experimental results can be qualitatively understood in terms of charge imbalance around phase-slip centers which nucleate at particular spots in the sample with a locally reduced transition temperature. [S0163-1829(98)05717-8]

I. INTRODUCTION

The superconducting properties of submicrometer-sized structures of aluminum have been the subject of intense studies in the past few years.[1] A number of surprising features have been found, which do not appear in bulk superconductors. Of particular interest are: (i) a pronounced enhancement of the resistance $R(T)$ above its normal-state value R_N close to the superconducting transition temperature T_c,[2–6] which is suppressed by a magnetic field of $\simeq$ 1–2 mT; (ii) in a magnetic field an increase of T_c is observed, suggesting that the resistance maximum occurs in the superconducting state[7] and, (iii) in loop structures, magnetoresistance peaks at fields differing from half-integer multiples of the superconducting flux quantum Φ_0, which are not expected from the classical Little-Parks effect.[3,4,6]

Very recently, an important aspect of the overshoots in $R(T)$ has been revealed: the anomaly can be suppressed by proper radio-frequency (rf) shielding of the electrical leads connected to the samples and reinduced by applying a rf signal.[7] In addition to the maxima in $R(T)$, excess voltages in the voltage-current characteristics, $V(I)$, have been found. The latter anomalies are very similar to those observed recently by Park *et al.*,[8] who investigated two-dimensional (2D) Al strips containing an artificially created normal/superconducting (N/S) interface.

An explanation in terms of nonequilibrium superconductivity was proposed,[7] which assumes the excitation of phase-slip centers (PSC's) by the rf irradiation. The PSC's are most easily induced at the weakest spots in the samples, where the transition temperature is reduced by a few mK due to unavoidable microstructural imperfections. The anomaly is located around such spots and is rapidly suppressed when the distance between the voltage probes is increased. This qualitative picture has recently been put into more quantitative terms by Arutyunov.[9]

A further complication of the situation arises from the finding of Burk *et al.*[10] that anomalies in $R(T)$ and $V(I)$ can also be obtained by adding an artificial ''noise'' current of intermediate frequency (1 kHz) to the low-frequency probe current. The latter results can in part be understood in terms of classical mixing of the extrinsic noise signal with the low-frequency measurement signal. The mixing is a simple consequence of the nonlinearity of the $V(I)$ characteristic near the critical current and is not a specific property of mesoscopic systems. The results of Refs. 7 and 10 point out that special care has to be taken to assure that the anomalies are not influenced or even induced by the presence of unintended noise sources.

In addition, resistance overshoots have been also reported near the superconducting transition of 2D films made of Al, granular In, CuZr metallic glasses and high-T_c materials.[11–15] An explanation for the anomalies measured in a *van der Pauw* configuration has been proposed by Vaglio *et al.*[16] Their interpretation is based on changes in the current distribution due to sample inhomogeneities when sweeping the temperature through the resistive transition. The latter kind of resistance anomalies is absent in one-dimensional (1D) structures, where the current path is uniquely defined.

In view of the broad range of observed effects and the variety of the proposed explanations, a separation of intrinsic and extrinsic anomalous effects is highly desirable. Even when filtering the electrical leads, a number of smaller artifacts are found in mesoscopic superconducting structures, which strongly vary from sample to sample and whose origin is difficult to identify. In this work, we restrict ourselves to effects, which are related to the 1D nature of our aluminum wires and have been consistently found in several samples.

The paper is organized as follows: in Sec. II we briefly discuss the different mechanisms which are candidates for an explanation of the anomaly in 1D structures. Experimental procedures are described in Sec. III. In Sec. IV results on the dependence of the rf-generated anomalies on the position of the voltage probes along the line are presented. In Sec. V we demonstrate that in the *absence of rf irradiation* the anomalous resistance peak also appears when the superconducting transition is measured with a sufficiently high dc current. We study the temperature and magnetic-field dependence of the anomalies. In Sec. VI we investigate the influence of a loop structure integrated into our wires. The transition tempera-

ture of the loop oscillates as a function of the applied magnetic field according to the Little-Parks effect.[17,18] Hence, the loop allows one to locally tune T_c by varying the magnetic field. In this experiment we can directly test the assumption that the anomaly arises around particular spots with a reduced transition temperature. Finally, in Sec. VII our experimental findings are discussed in the framework of related experimental and theoretical work.

II. MODELS

The most striking feature of the anomalous effects described in this paper is the observation of a resistance R that can be substantially larger than the normal state resistance R_N. More general, excess voltages $V_{\rm ex}=V-R_N I$ are present which can be detected both via the resistance $R(T)$ and the current-voltage characteristics $V(I)$. According to the BCS theory, many quasiparticles are thermally excited above the energy gap when T is close to the zero-field transition temperature T_{c0}. As the superconducting state is destroyed above T_{c0}, voltages develop in the metallic wire and the quasiparticles dominate the electrical transport. Above T_{c0}, Aslamasov-Larkin and Maki-Thompson fluctuations contribute to the conduction process and reduce the resistance below the normal-state value.[19] For our relatively clean films, phenomena such as electron localization and the Kondo effect can be excluded as a possible origin of the sharp resistance peaks close to T_{c0}. Hence, it appears that the excess voltages are generated directly at the transition or even in the superconducting state.

A simple model to explain the resistance anomaly relies on the nonlinearity of the voltage-current characteristics near the critical current.[10] According to standard Fourier analysis, the superposition of the low-frequency (ω_p) or dc ($\omega_p=0$) probe current with a noise current of different frequency ($\omega_{\rm noise}$) leads to a component in the response voltage at the frequency ω_p of the probe current which is determined by the amplitude of the *noise current*. Roughly speaking, the strongly nonlinear region of the current voltage characteristics with $dV/dI \gg R_N$ is probed, when the noise current amplitude becomes comparable to the critical current. Since this classical mixing effect is independent of $\omega_{\rm noise}$, potential extrinsic noise sources range from the 50 Hz line frequency up to the AM and FM radio-frequency regime.

A more intrinsic explanation of the enhanced resistance in the superconducting state relies on nonequilibrium superconductivity.[12] According to the Josephson relation $\hbar\partial\phi/\partial t=-2\mu_p$ any voltage drop $\Delta\mu_p/e$ generated in the superconducting state is accompanied by a time dependence of the superconducting order parameter $\Psi(t)=|\Psi(t)|\exp(i\phi(t))$, where μ_p denotes the Cooper pair electrochemical potential. In the case of 2D superconducting films in perpendicular magnetic fields this time dependence can be induced, e.g., by the motion of vortices. Vortices are absent in our structures because, close to the mean-field transition temperature T_{c0}, both the superconducting coherence length $\xi(T)=\xi_{\rm GL}/(1-T/T_{c0})^{-1/2}$ and the magnetic penetration depth $\lambda(T)$ are much larger than the width d of the superconducting strands. For the same reason we have nearly complete field penetration in the superconducting strands and the difference between the magnetic induction B and the applied magnetic field $\mu_0 H$ is small. In the case of long 1D wires, it has been established that the onset of resistive behavior occurs through phase slip processes. Close to T_c, the phase slip can be thermally excited as described by the theory of Langer and Ambegaokar[20] and its refinement by McCumber and Halperin.[21] The thermally activated phase slip provides a dissipation mechanism below T_c but does not explain a resistance $R>R_N$.[22]

At slightly lower temperatures, where the thermal activation becomes less and less important, the phase slip does not occur in a random fashion but in a time-periodic cycle in so-called phase-slip centers. When the current exceeds the local critical current, $\Psi(x,t)$ breaks down and the current is taken over by the quasiparticles. Consequently, $\Psi(x,t)$ builds up again, the superconducting condensate being accelerated by the applied voltage until the critical current is exceeded and the whole cycle starts again. The classical signature of PSC's in long wires are steps in the current voltage characteristic $V(I)$ with a constant differential resistance dV/dI in between the steps. The differential resistance increases by the same amount for each step, which corresponds to the nucleation of a new phase-slip center.[23,24] This phenomenon is well described by the model of Skocpol, Beasley, and Tinkham (SBT).[25] In a core region of length $\simeq 2\xi(T)$ the time-averaged amplitude of the superconducting order parameter $|\Psi(x)|$ is reduced and the phase difference between the fractions of the condensate on both sides of the PSC oscillates with the Josephson frequency. Since the amplitude of the order parameter oscillates in time, a continuous conversion from Cooper pairs to quasiparticles is required. Due to the finite time $\tau_{Q*}(T)$ necessary for transitions between the quasiparticle system and the superconducting condensate, a region of charge imbalance is formed, in which the time averages $\langle\mu_p(x)\rangle$, $\langle\mu_q(x)\rangle$ of the Cooper pair and the quasiparticle electrochemical potential are different (see Fig. 1). While $\langle\mu_p(x)\rangle$ shows a sharp drop in the core region and is constant outside the core, $\langle\mu_q(x)\rangle$ varies on the scale $\Lambda_{Q*}=\sqrt{D\tau_{Q*}}$, where $D=v_F l_{\rm el}/3$ is the electronic diffusion constant, v_F is the Fermi velocity, and $l_{\rm el}$ is the elastic mean free path. The charge imbalance length Λ_{Q*} determines the distance over which the condensate and the quasiparticle system get back in equilibrium. For our samples Λ_{Q*} is several times larger than $\xi(T)$. Outside the nonequilibrium region, i.e., far away from the PSC, $\mu_p(x)$ and $\mu_q(x)$ are equal and the voltage drop across the PSC is given by

$$V_\infty = 2\Lambda_{Q*}(T)\rho_N(I-\langle I_S\rangle), \tag{1}$$

ρ_N being the normal-state resistance per unit length and $\langle I_S\rangle$ the time-averaged supercurrent at the core of the PSC.[25] For comparison, Fig. 1 also includes the linear variation of the quasiparticle potential above T_c (denoted by $\mu_{\rm normal}$). The slope of $\langle\mu_q(x)\rangle$ is reduced near the core with respect to the slope of $\mu_{\rm normal}$ because of the nonzero value of $\langle I_S\rangle$ at the core.

Refinements of the SBT model have been proposed by Kadin *et al.*,[26] by Ivlev and Kopnin[27,28] and by Baratoff.[29] Kadin *et al.* have found that propagating waves of charge imbalance can be excited at the PSC and identified an intrinsic mechanism of hysteresis in the $V(I)$ characteristics. Ivlev and Kopnin and also Baratoff have calculated that $|\Psi(x)|$

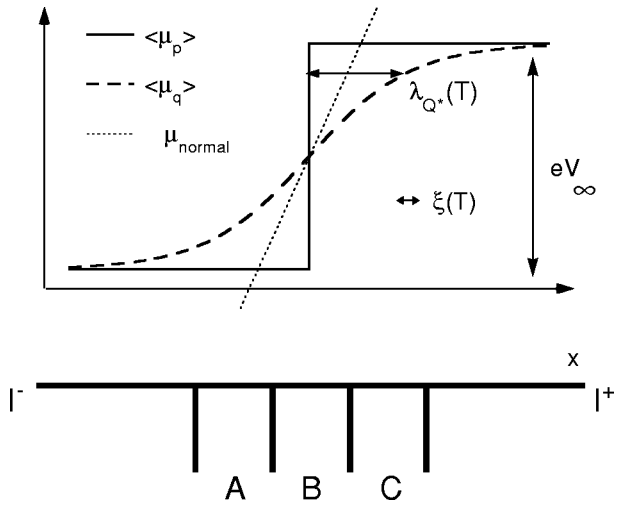

FIG. 1. Schematic plot of the variation of the time-averaged electrochemical potentials μ_q and μ_p vs x in the nonequilibrium region around a phase-slip center. The dash-dotted line indicates the quasiparticle electrochemical potential $\mu_{\rm normal}$ in the normal state.

shows not only a time-dependent variation during the phase-slip cycle but in addition a time-independent, static depression in the vicinity of the core, which results in a decoupling of the core of the PSC from the wings, where the charge imbalance relaxes towards equilibrium. Such a decoupling has been observed by Liengme *et al.*, who studied very homogeneous thick Al wires.[30] Remarkably, the SBT predictions for the spatial dependence of $\langle \mu_q(x) \rangle$ turned out to be nearly identical to those of the more detailed model calculations:[28]

$$\langle \mu_q(x) \rangle = e \Lambda_{Q*} \rho_N (I - \langle I_S \rangle) \tanh((x - x_{\rm psc})/\Lambda_{Q*}), \quad (2)$$

where $x_{\rm psc}$ denotes the position of the core of the PSC. In contrast, $\langle \mu_p(x) \rangle$ is expected to drop discontinuously at $x_{\rm psc}$. This result (see the schematic in Fig. 1) has been verified experimentally by Dolan and Jackel[31] for tin and indium wires and later by Stuivinga *et al.*[32] for Al wires. $\langle \mu_p(x) \rangle$ and $\langle \mu_q(x) \rangle$ have been measured using superconducting and normal voltage probes, respectively. While the relatively slow decay of $\langle \mu_q(x) \rangle$ on the scale of Λ_{Q*} could be well resolved, the fast drop of $\langle \mu_p(x) \rangle$ at the core occurred on a scale shorter than the spacing of the potential probes, i.e., $\lesssim 2$ μm $\approx \xi(T)$. In general, the drop in $\langle \mu_p(x) \rangle$ measured with superconducting probes is expected to be essentially independent of the probe spacing Δx [at least for $\Delta x \gtrsim \xi(T)$]. From Eq. (1) one obtains an apparent resistance $R(T) > R_N$

$$R(T) = 2 \Lambda_{Q*}(T) \rho_N (1 - \langle I_S \rangle / I) > \Delta x \rho_N \quad (3)$$

when measuring with superconducting voltage probes just across the core of the PSC. Since $\langle I_S \rangle \simeq 0.5 I_c(T)$ (see Refs. 25,32) the latter inequality is valid for $\Delta x \lesssim \Lambda_{Q*}$ and $I \simeq I_c$.

The most important parameter in the phase-slip model is the charge imbalance length Λ_{Q*}, which can be obtained from the theory of Schmid and Schön.[33] This theory provides expressions for the charge imbalance relaxation time τ_{Q*} for various pair breaking mechanisms:

$$\tau_{Q*} = \frac{4 k_B T}{\pi \Delta(T,B)} \sqrt{\frac{\tau_E}{2\Gamma}}. \quad (4)$$

The inelastic scattering time τ_E depends on disorder[34] and was estimated to be about 4 ns for thin Al films[32] ($t \simeq 50$ nm), while for thicker films ($t \simeq 400$ nm) $\tau_E \simeq 12$ ns has been found.[35] Δ is the superconducting order parameter $\Delta(T,B) = \Delta(T)[1 - B^2/B_c^2(T)]^{1/2}$ (see Ref. 36), $B_c(T)$ being the critical field, and

$$\Gamma = \frac{1}{\tau_s} + \frac{1}{2\tau_E} + \frac{D}{2}\left(\frac{4 m^2 v_s^2}{\hbar^2} - \frac{1}{\Delta} \frac{\partial^2 \Delta}{\partial x^2} \right). \quad (5)$$

The first term in Eq. (5) describes the effect of orbital pair-breaking and spin-flip scattering, the second describes the effect of inelastic scattering, the third pair breaking by the supercurrent and, the last term describes the effect of spatial variation of the gap parameter Δ near the core of the PSC. v_s is the superfluid velocity. For $\tau_E \simeq$ 4 ns the contributions of the third and fourth term in Eq. (5) were found to be negligible in Al.[32,37] In the absence of paramagnetic impurities and close to T_{c0} τ_s is given by[36]

$$\tau_s(T,B) = \frac{\hbar}{\Delta(0,0)} \frac{B_c^2(0)}{B^2} = \frac{\pi \hbar}{8 k_B [T_{c0} - T_c(B)]}. \quad (6)$$

Equation (4) predicts a decay of $\Lambda_{Q*} = \sqrt{D \tau_{Q*}}$ and, consequently, a suppression of the excess voltages in a magnetic field.

Although phase-slip processes have been studied for many years, no resistance anomalies or excess voltages were reported at that time and it was understood only recently[7–9] that PSC's may play a central role for the appearance of the anomalies in mesoscopic samples. In the course of our investigation we shall see that the charge imbalance around PSC's may provide an explanation for many but not all of our experimental observations.

III. EXPERIMENTAL

Samples were prepared by thermal evaporation of 99.999% pure Al onto oxidized Si wafers. The patterns were defined using a bilayer PMMA resist and standard electron beam lithography methods. Scanning electron and atomic-force microscopy (AFM) ensured a smooth Al surface with no major cracks or holes down to the nanometer scale. The film thickness varied between 25 and 45 nm. Some series of samples have been evaporated onto liquid-nitrogen cooled substrates. In the latter case, a higher residual resistivity has been obtained, leading to a smaller amplitude of the anomalies but not to qualitative changes.

Two kinds of structures have been studied. Figure 2(a) shows an AFM micrograph of a line structure of 0.2 μm width (to which we will refer below as structure A) with a number of equidistant voltage probes with 1 μm spacing. This design allows us to map out the spatial dependence of the anomalies emerging in our 1D wires. We show data for two samples of type A labeled A1 and A2, respectively. To investigate the influence of an artificial tunable inhomogeneity, 0.14 μm wide line samples containing a square loop of 1 μm outer sidelength have been prepared [see structure B in

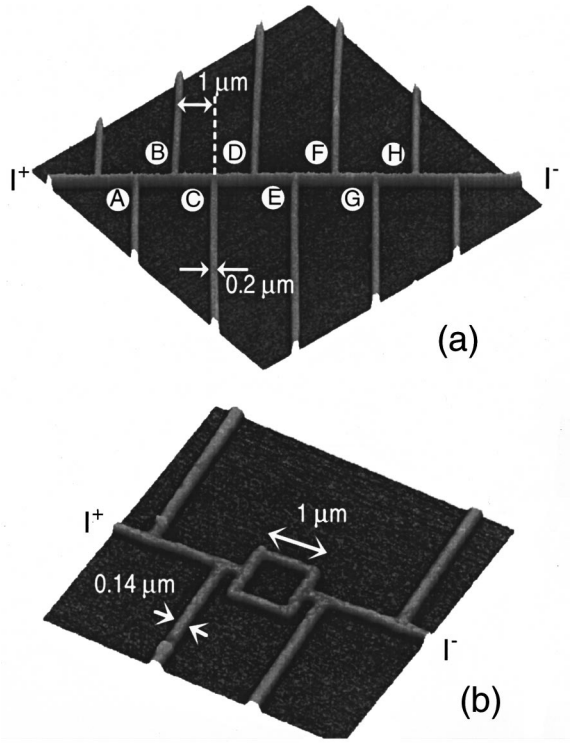

FIG. 2. AFM micrograph of (a) sample A1 with multiple voltage probes and (b) sample B1 containing a loop.

Fig. 2(b)]. A perpendicular magnetic field allows one to locally depress $|\Psi|$ and the transition temperature in the loop for samples of type B.[38] The structural and electrical parameters of the samples are listed in Table I. The width of the current and voltage leads is kept constant at 0.2 and 0.14 μm, respectively, to a distance of 7 μm from the sample in order to minimize the influence of the wide parts of the contacts on the measurement. The magnetic field is always applied perpendicular to the sample. Figure 3(a) shows a detail of the AFM micrograph in Fig. 2(a) displaying three segments of the line. The picture confirms the smoothness of the metallic wire with no apparent structural defects in any of the different segments. The structural homogeneity of our samples is further illustrated in Fig. 3(b) where the height profile of the same segment of the sample is plotted. The thickness of the polycrystalline film varies by about 2 nm, the grain size being about 30 nm, typical for a polycrystalline Al film of this thickness. Since the grain size is a factor of 5–8 smaller than the width of the wires d, it is unlikely that the grain structure causes sample inhomogeneities on the scale of d.

The transport measurements were performed with a PAR 124A lock-in amplifier for ac measurements at 27 Hz. In addition, $V(I)$ curves have been measured using a HP 34420A dc nanovoltmeter. All electrical leads have been shielded by π filters with a cutoff frequency of 1 MHz. Special care has been taken to also exclude the presence of parasitic ac signals at lower frequencies which may mix into the measuring signal due to the highly nonlinear $V(I)$ characteristics near the superconducting transition. The residual noise was always far below the level which is necessary to trigger the effects described in Ref. 10. The rf signal was supplied to the sample with two coaxial cables in a separate tube and close to the sample capacitively coupled to the current leads (see Fig. 4). Because of the changing impedance of the sample as it goes through the superconducting transition, one cannot avoid an impedance mismatch between the sample and the rf source and it is difficult to control the actual amount of rf power injected into the sample. A part of the rf power is also lost through the capacitance of the π filters in the measuring leads, resulting in a monotonic decrease of the rf current from the end of the sample connected to the rf source towards the grounded end of the sample. We can interchange the injection side and the grounded side to check for features independent of the injection point of the rf power. The normal-superconducting phase boundaries have been measured by tracing the midpoint temperature of the resistive transition with the aid of a feedback technique while ramping slowly the magnetic field. The temperature stability of the feedback circuit was about 0.1 mK.

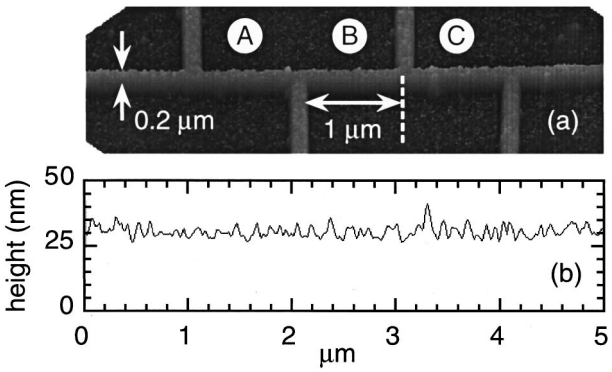

FIG. 3. (a) Detail of Fig. 2(a) with the segment B showing the anomaly and its two neighboring segments A and C. (b) Height profile along the center of the wire for the same part of the sample. Note that the scale for the x axis is strongly compressed when compared to the scale for the y axis.

IV. ANOMALIES INDUCED BY RF INTERFERENCE

Before exposing the samples to significant external disturbances let us first look at the resistive transition curves when the measuring current is small. Figure 5 shows the resistive

TABLE I. Material parameters for the measured samples of type A and B. Identical parameters for all samples are: $\rho \cdot l_{el} = 4 \times 10^{-16}$ Ω m^2 (see Ref. 50), $v_F = 1.3 \times 10^6$ m/s, $\xi_{GL} = 0.86\sqrt{\xi_0 l_{el}}$ and, $\xi_0 = 1.6$ μm.

Sample	t(nm)	d(nm)	$R_N(\Omega)$	$\rho(\mu\Omega$ cm)	l_{el}(nm)	D(cm^2/s)	T_{c0}(K)	ξ_{GL} (μm)
A1	30	200	6.4	3.8	11	48	1.372	0.13
A2	30	200	7.5	4.4	9.4	41	1.373	0.12
B1	43	140	$8.4^{(loop)}(5.5^{(lead)})$	2.3	16	70	1.294	0.14

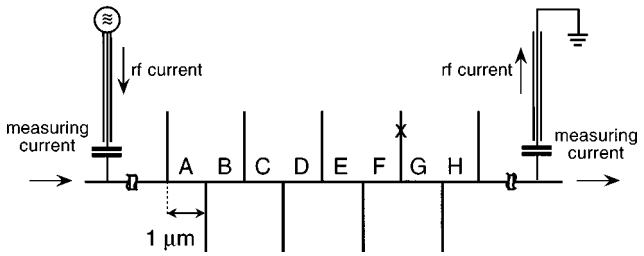

FIG. 4. Schematic of the lead configuration for applying a rf signal. The crossed voltage probe of sample A1 burned out before performing the rf measurements.

transition of the different segments of sample A1 of type A. The segments are labeled from A to H from the left to the right [see Fig. 2(a)]. In addition to the $R(T)$ curves of the individual segments, we have included the transition curve measured with the two outermost voltage probes. The resistance of the latter curve has been divided by the number of segments to facilitate the comparison with the single segments. Except for small differences in T_c in the outermost segments A and H, the curves fall on top of each other. The normal-state resistance values deviate by a few percent due to the geometric tolerances of the lithographic patterning process.

Figure 5 confirms the homogeneity of the sample in the case of small ac measurement currents of about 100 nA. We will show below that strong differences in the behavior of the individual segments appear when the sample is subjected to either a rf current or a higher dc current. Note the absence of any resistance anomaly in all of the segments. The rounded top of the transition is well described by the contribution of Aslamasov-Larkin fluctuations which dominate the conductivity of our 1D samples very close to T_{c0}. From a fit of the Aslamasov-Larkin formula[19] to the data (see the inset

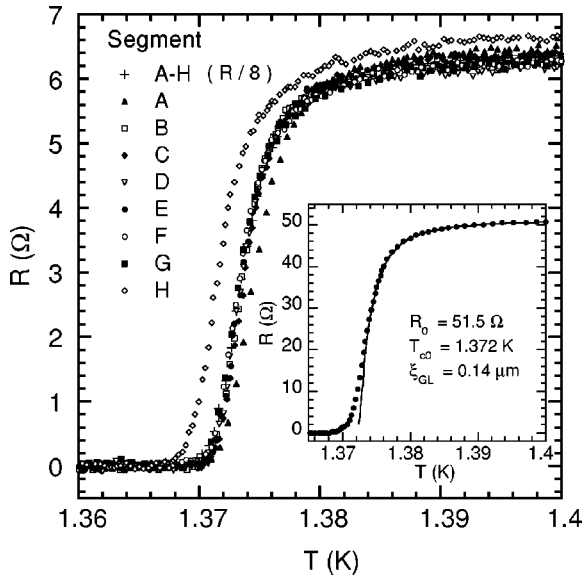

FIG. 5. $R(T)$ curves for different segments of sample A1 of type A in absence of rf irradiation. The resistance values of the R(T) curve for the combined segments A-H has been divided by the number of segments. Inset: Transition curve for the combined segments A-H together with a fit according to the Aslamasov-Larkin formula.

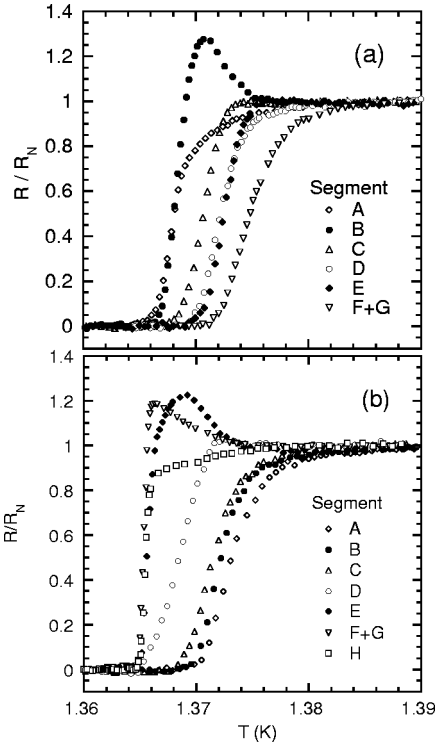

FIG. 6. $R(T)$ curves for different segments of sample A1 with a rf signal of 850 MHz frequency and −30 dB power applied. (a) Injection of the rf current via the left-hand current lead. (b) Injection of the rf current via the right-hand current lead (see the sample layout in Fig. 4).

in Fig. 5) we obtain $T_{c0} = 1.372 \pm 0.001$ mK. The measuring current of 100 nA gives rise to a small reduction of T_c of the order of 1–2 mK. The fit also yields $\xi_{GL} \simeq 0.14$ μm in reasonable agreement with the values in Table I.

The experimental observation that the resistance anomalies can be suppressed by suitable rf filtering leads to the idea to induce the anomalies in a controlled way by irradiating the samples with an external rf source.[7] When irradiating the sample shown in Fig. 5 with a rf signal, pronounced resistance anomalies appear in certain segments of the sample. Figure 6(a) shows the $R(T)$ curves for the sample at the same ac measurement current, but in the presence of a −31 dBm rf power at a frequency of 850 MHz. The height of the resistance peak varies nonmonotonically with increasing distance from the rf injection point at the left-hand side (see the schematic in Fig. 4). The strongest anomaly is found in segment B while another smaller anomaly is visible again in segment E. When the rf injection point is switched to the current lead at the right-hand side, the peak at segment E becomes the dominating anomaly while the peak at segment B vanishes [see Fig. 6(b)]. The reason for this is that rf power is lost along the sample, mainly due to the capacitance of the π filters in the voltage leads. The anomalies appear at certain ''active'' spots in the sample, which are independent of the injection point of the rf power but vary from sample to sample. Note that two active spots have been identified in this sample.

Relying on our structural characterization, we can exclude local variations of the cross section as a possible cause of the drastically varying behavior of the different segments (see

Fig. 3). No significant structural differences are found between segment B (showing a pronounced anomaly) and the adjacent segments. The effect of the rf irradiation is twofold: (i) a depression of the transition temperature due to heating or pair breaking and, (ii) the generation of the resistance peak at specific spots within the sample. Similar behavior is found in the frequency interval between 100 MHz and 2 GHz. We cannot compare the results obtained at different frequencies, since the impedance matching problems mentioned above prevent a control of the rf amplitude applied to the sample.

In our previous work,[7] we have also observed a modification of the $V(I)$ curves in the presence of the rf irradiation. An enhanced slope dV/dI near $I=0$ is directly related to the resistance maximum. At lower temperatures the enhanced slope develops into a pronounced maximum in $V(I)$ close to the critical current (see Fig. 4 in Ref. 7). The decrease in $V(I)$ after the maximum corresponds to a locally *negative* differential resistance. As explained in Sec. II, the excess voltages in $V(I)$ can be interpreted in terms of a charge imbalance effect in the vicinity of PSC's which are induced by the rf irradiation. This interpretation is consistent with previous experiments on long Sn wires,[39] which have demonstrated that PSC's can indeed be created by rf irradiation.

V. ANOMALIES INDUCED BY A dc CURRENT

How can we distinguish between the effects described in Sec. IV and the classical mixing of the rf signal and the low-frequency measuring signal? Besides the bump in $R(T)$, the mixing also induces an enhancement of the differential resistance above R_N near zero bias current which disappears as the temperature is decreased.[10] In contrast to the rf-induced anomalies, dV/dI is expected to remain always positive for a simple mixing mechanism.

Subjecting the sample to higher dc currents rather than a rf field can help to separate the possible mixing effects and the intrinsic effects related to nonequilibrium superconductivity: if a classical mixing effect is involved, no anomalies should be induced by a dc current. On the other hand, PSC's are usually studied using dc currents rather than by applying rf irradiation. When the dc current is increased while the temperature is kept constant, phase-slip centers are expected to nucleate at the spots with the lowest critical current. If phase-slip processes are indeed related to the appearance of the anomalous excess voltages, the nucleation of a PSC should lead to the same nonmonotonic $V(I)$ curve which is observed under rf irradiation. Conversely, when the current is kept fixed and the temperature is raised, I_c decreases and an anomaly should emerge for $I_{\rm dc}\simeq I_c(T)$. Figure 7 shows the $R(T)$ curves of segment B of sample A1 (see Fig. 4) for a variety of dc currents. For the lowest current of 0.1 μA no anomaly is seen and the curve agrees well with the corresponding ac measurement shown in Fig. 5. With increasing dc measuring current, however, a shoulder is gradually developing at the top of the transition, which turns into a pronounced maximum at about 0.5 μA, and clearly exceeds R_N at $I_{\rm dc}=$ 0.6 and 0.7 μA.[40] The current necessary for the generation of the anomaly varies from segment to segment as well as from sample to sample. We have checked the presence of dc current-induced bumps for the other segments of sample A1 and found another pronounced anomaly on segment E. Hence, for the same sample both the dc current and the rf irradiation create the anomaly at the same particular spots.

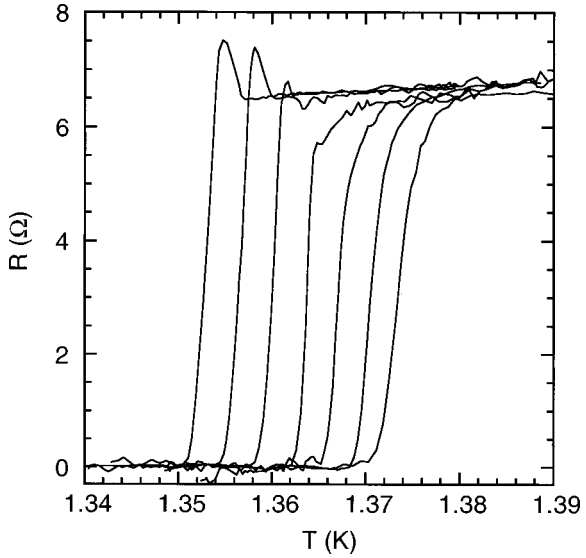

FIG. 7. $R(T)$ curves for segment B of sample A1 for different values of the dc current. The current values are from the left to the right: 0.7, 0.6, 0.5, 0.4, 0.3, 0.2, and, 0.1 μA.

Another important consequence of the phase-slip scenario comes from the fact that the sharp drop in $\langle \mu_p \rangle$ at the PSC is caused by the Josephson effect in the core of the PSC and it should obey the Josephson relation. This implies that $\langle \Delta \mu_p \rangle$ is independent of the distance L between the voltage probes, certainly when $L \gtrsim \xi(T)$. Since the voltage drop in the normal state is given by $R_N \propto L$, the anomaly is expected to be completely masked by the rapid increase of $V(I)$ at the transition when L and R_N are large. This effect is demonstrated in Fig. 8 where the voltage-current characteristics for seg-

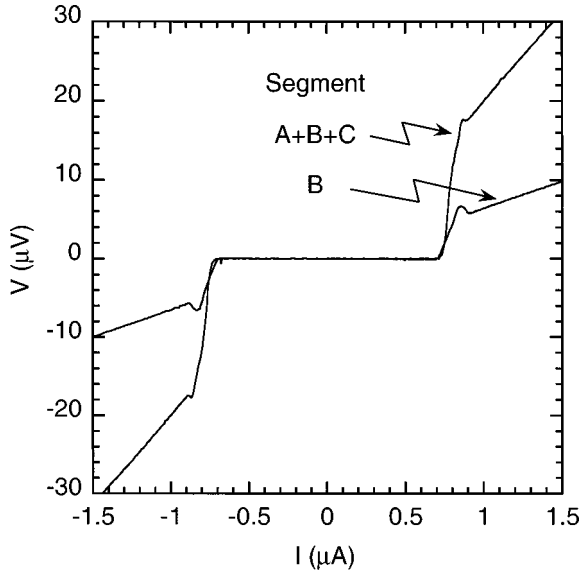

FIG. 8. Nonmonotonic $V(I)$ curves for segment B as well as for the combined segments A, B, and C of sample A1 at $T=1.352$ K. Note that the anomaly is strongly reduced when the distance between the voltage probes is increased.

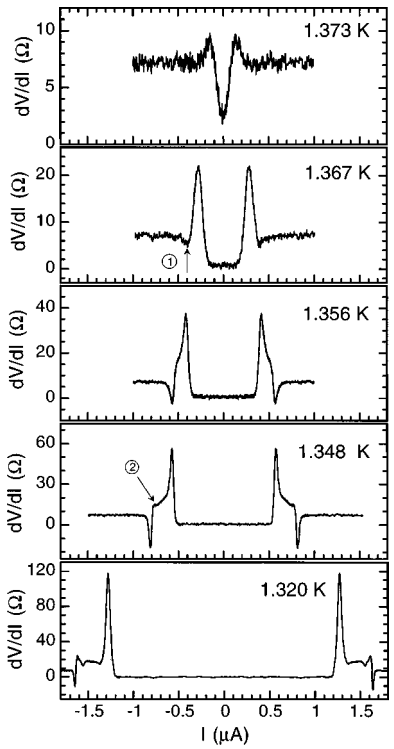

FIG. 9. Temperature dependence of $dV/dI(I)$ for segment C of sample A2, which shows a dc current induced bump in $R(T)$.

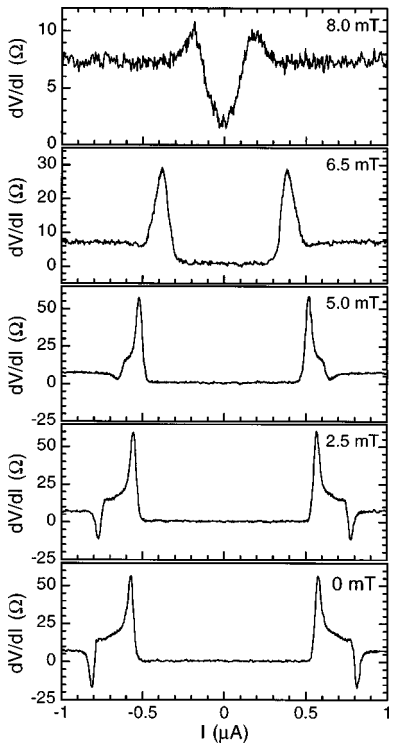

FIG. 10. Magnetic-field dependence of $dV/dI(I)$ for the same segment of sample A2 at $T=1.348$ K.

ment B and the combined segments A+B+C are plotted. The pronounced anomaly for segment B is strongly reduced when measuring with larger probe distance, in agreement with the earlier observations of Santhanam *et al.*[2] In order to separate the current and the temperature dependence, we present in the rest of this section measurements as a function dc bias current. Many important quantities like $\xi(T)$, $\Lambda_{Q*}(T)$, $I_c(T)$, etc. can then be kept constant. We also switch to dV/dI measurements, to obtain a better signal-to-noise ratio.

Figure 9 illustrates the evolution of the anomalous dV/dI curves as a function of temperature. The data are obtained on sample A2 using an ac probe current of 10 nA. The anomaly manifests itself as an initial decrease of dV/dI as $|I_{\rm dc}|$ is decreased from $|I_{\rm dc}|>I_c(T)$. At $T=$ 1.373 K an ordinary dV/dI curve is obtained which only shows the regular peak corresponding to the enhanced slope of $V(I)$ at the critical current. At $T=1.367$ K a small dip (see arrow 1) in dV/dI emerges, related to an increase of $V(I)$ above the Ohmic straight line. As the temperature is decreased further, this dip becomes more and more pronounced, developing into a strongly negative differential resistance spike. The locally negative differential resistance is directly related to the non-monotonic $V(I)$ curves discussed above. At the lowest temperatures, a shoulder (see arrow 2) appears in dV/dI, which evolves into a second (smaller) maximum in dV/dI at $T=1.320$ K. This shoulder appeared in some, but not all of our samples and is also observed in the experiments by Park *et al.*[8] The integrated dV/dI curves coincide very well with the directly measured $V(I)$ curves. The increasing height of the dV/dI maxima reflects the increase of the critical current when decreasing the temperature. If the dip in $V(I)$ would be caused by mixing of the measuring current with any spurious noise current $I_{\rm noise}$, one would expect that the anomaly becomes more pronounced when $I_{\rm noise}/I_c(T)$ increases. Assuming then a fixed amplitude of $I_{\rm noise}$, the anomaly should grow with increasing temperature, i.e., decreasing I_c, which is inconsistent with our experimental observations.

To further check the validity of the phase-slip picture we have also measured the behavior of the anomaly in a magnetic field. Because $\langle\Delta\mu_p\rangle\propto\Lambda_{Q*}\propto\sqrt{\tau_{Q*}}$ [Eq. (1)] one would expect a suppression of the anomaly with increasing field since the magnetic field reduces the charge imbalance relaxation time τ_{Q*} due to orbital pair breaking.[33,36] In Fig. 10 the dV/dI curves are plotted for magnetic fields ranging from 0 to 8.5 mT. The temperature is kept constant at 1.348 K, corresponding to $\Delta T=T_{c0}-T=25$ mK. A magnetic field of 5 mT strongly reduces the anomalous negative differential resistance peak while the positive peak remains nearly unaffected. The latter observation indicates that the critical current is only slightly suppressed by a magnetic field of 5 mT. For magnetic fields close to the critical field of about 8 mT, I_c also tends towards zero and regular dV/dI curves are recovered. For comparison, Fig. 11 shows the theoretical behavior of $\tau_{Q*}(B)$ and $\Lambda_{Q*}(B)$ computed from Eq. (4) with the sample parameters listed in Table I. The same magnetic field of 5 mT that suppresses the negative dV/dI spikes (see Fig. 10) reduces τ_{Q*} by a factor of 5 (see the 25 mK trace in Fig. 11). At higher fields, τ_{Q*} saturates and eventually raises again due to the vanishing of $\Delta(T,B)$ close to the second-order phase transition at $T=T_c(B)$ [see Eq. (4)]. As in zero field, however, this divergence of τ_{Q*} does not lead to a reappearance of the anomaly close to the phase boundary. The possible origin for the absence of anomalies in dV/dI close to the phase boundary will be discussed below.

We conclude this section by noting that, in the absence of

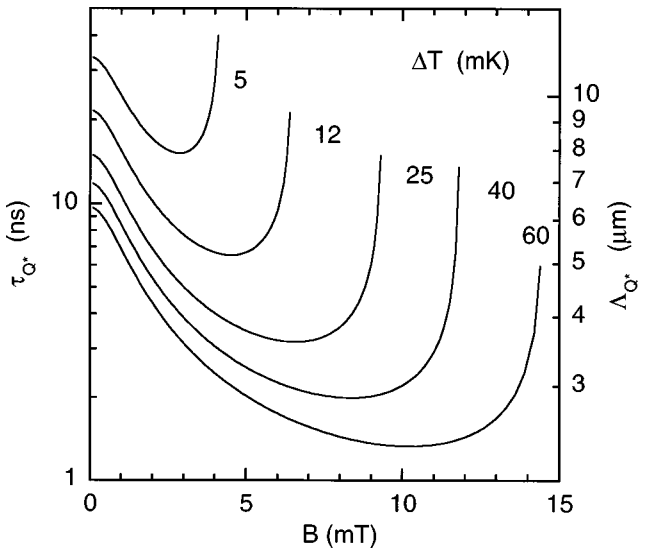

FIG. 11. Charge imbalance relaxation time τ_{Q*} vs magnetic field for various values of $\Delta T = T_{c0} - T$. Curves are calculated from Eq. (4) using the parameters of sample A2 in Table I. The 25 mK trace corresponds to the temperature at which the data in Fig. 10 were recorded.

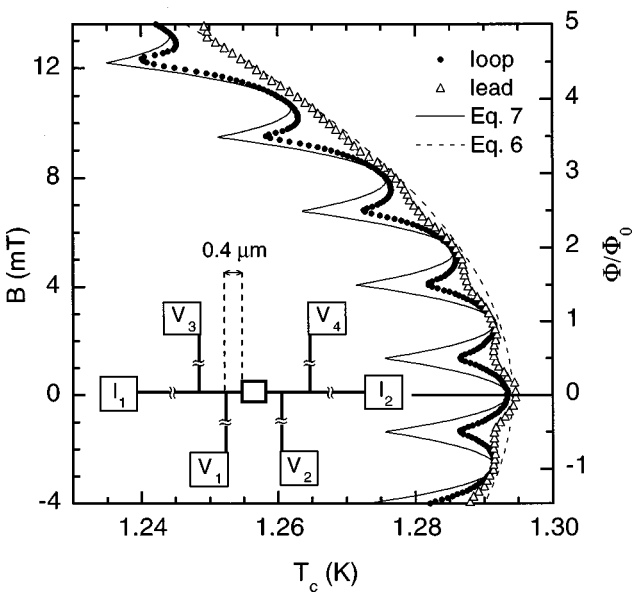

FIG. 12. Magnetic phase boundaries $T_c(B)$ for the loop segment (voltage contacts $V1/V2$) and a lead segment (voltage contacts $V1/V3$) of sample B1 [see also Fig. 2(b)]. Dashed and solid lines are fits according to Eqs. (7) and (8), respectively

rf interference, anomalies in both $R(T)$ and $V(I)$ can be induced by a pure dc current. The similarity of the rf and the dc current-induced effects and the fact that both effects appear for the same segments of the sample, strongly indicate that the same underlying mechanism is responsible for the anomalies.

The remaining question is: why do the anomalies appear only at specific positions which vary from sample to sample? In previous experiments on PSC's the energy gap along superconducting strips has been measured with tunneling spectroscopy.[32,41] It was found that small local variations of T_c and Δ determine the ''weakest'' spot of the superconductor, where phase slipping preferentially occurs. The transition temperature of Al is known to strongly depend on the oxygen content and the presence of structural defects. In our Al samples, T_{c0} is indeed slightly enhanced above the bulk T_c value of 1.19 K. Hence, inhomogeneities in T_{c0} could originate from small local variations of the oxygen content or the defect concentration and would be most important very close to T_{c0} where the order parameter strongly depends on T.

VI. MAGNETIC FIELD-INDUCED ANOMALIES IN LOOP STRUCTURES

Experiments on loop structures are suitable to test the hypothesis that spots of a locally reduced T_c [implying a locally reduced $\Delta(T)$ and $I_c(T)$] are the preferred locations for the appearance of the anomaly. In our structures of type B [see Fig. 2(b)] the superconducting wire is interrupted by a loop. The Little-Parks (LP) effect[17] in this loop can be used to reduce T_c near the loop by varying the magnetic flux Φ threading the loop.

For mesoscopic wires with width $d \lesssim \xi(T)$, the Tinkham formula for the critical field of thin films in a parallel magnetic field[19] becomes also valid for a perpendicular field, provided that the film thickness t is replaced by the width d of the wire:

$$T_c(B) = T_{c0}\left[1 - \frac{\pi^2}{3}\left(\frac{d\xi_{\mathrm{GL}}B}{\Phi_0}\right)^2\right]. \tag{7}$$

When the wire is bent into a closed loop, fluxoid quantization requires the presence of a screening current that oscillates with the magnetic flux Φ threading the loop. Consequently, the transition temperature $T_c(B)$ oscillates with the magnetic field B. These Little-Parks oscillations are superimposed with the monotonic background suppression of T_c given by Eq. (7):[18]

$$T_c(B) = T_{c0}\left\{1 - \left(\frac{\xi_{\mathrm{GL}}}{R_m}\right)^2\left[\left(\frac{\pi R_m^2 B}{\Phi_0}\right)^2 (1+z^2) - 2n\frac{\pi R_m^2 B}{\Phi_0} + \frac{n^2}{2z}\ln\left(\frac{1+z}{1-z}\right)\right]\right\}. \tag{8}$$

Here $R_m = (R_{\max} + R_{\min})/2$ is the average of the inner and outer radius of the loop, where $d = R_{\max} - R_{\min}$ is the width of the wire and $z = d/2R_m$ the loop aspect ratio. The integer n has to be chosen such that $T_c(B)$ is maximized for a given value of B.

We have recently reported that the LP effect of a loop connected to electrical leads differs from that of an isolated loop or a microcylinder in an axial magnetic field.[42] Figure 12 shows the magnetic-field dependence of the critical temperature of the loop segment (voltage probes V_1/V_2) as well as of a segment of the current leads (voltage probes V_1/V_3) at a distance of 0.4 μm from the loop. $T_c(B)$ corresponds to the point of the transition curve where $R(T,B) = R_N/2$. At low magnetic fields the amplitude of the LP oscillations in the loop is reduced, while $T_c(B)$ for the lead segments reveals an oscillatory component. The solid line in Fig. 12 represents the case of the classical LP effect for an isolated

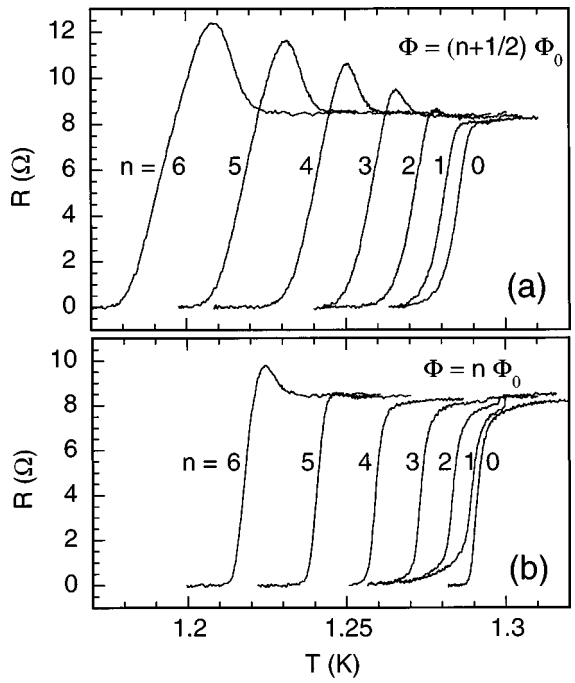

FIG. 13. $R(T)$ curves of the loop segment of sample B1 for (a) *half-integer* and (b) *integer* values of Φ/Φ_0.

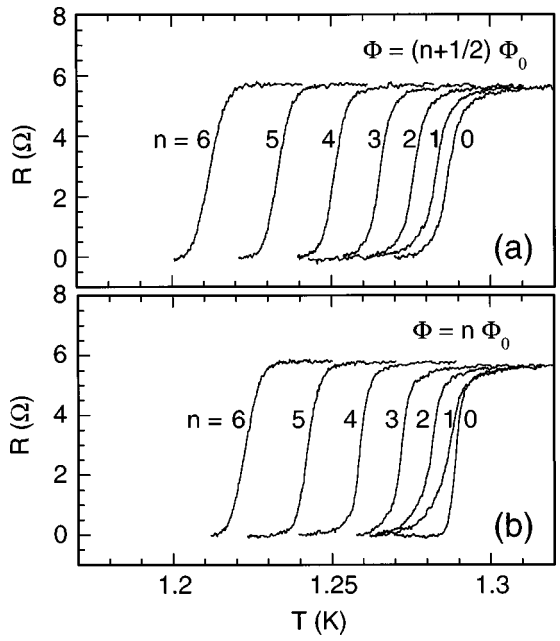

FIG. 14. $R(T)$ curves of the lead segment of sample B1 for (a) *half-integer* and (b) *integer* values of Φ/Φ_0.

loop. Equation (8) implies that the oscillatory part of $T_c(B)$ has a constant amplitude θ_0 [$\theta_0 = T_{c0}(\xi_{GL}/2R_m)^2 \simeq 18$ mK for sample B1]. While R_m can be accurately determined from the period of the oscillations, the value of ξ_{GL} is provided by fitting Eq. (7) to the envelope of the measured phase boundary of the loop segment. Since R_m and ξ_{GL} are determined independently θ_0 is not a free parameter. The behavior of a straight wire [(Eq. (7)] is indicated by the dashed line in Fig. 12.

As seen in Fig. 12 in our case of a loop with leads attached, the difference $\Delta T_c = T_c^{(lead)} - T_c^{(loop)}$ oscillates with an amplitude θ that grows with increasing values of Φ/Φ_0. For small Φ/Φ_0, θ is only 3–4 mK while θ approaches θ_0 at higher Φ/Φ_0. We believe that the increase of θ is a consequence of the decrease of the coherence length $\xi(T_c(B))$ at the phase boundary[42] at higher magnetic fields, where the finite width of the arms of the loop causes a background suppression of $T_c(B)$. As $\xi(T)$ decreases, the coupling between the loop and the leads is reduced. Accordingly, the oscillation amplitude of $T_c(B)$ in the loop tends towards the value θ_0 for an isolated loop, while the nonlocal oscillation of $T_c(B)$ for the lead segment vanishes (see Ref. 42 for further details).

In order to link the emergence of a resistance peak near T_c to a local reduction of T_c, we now look in detail at the shape of the resistive transition as a function of the magnetic flux threading the loop. In Fig. 13 the $R(T)$ curves for the loop segment [voltage contacts $V1/V2$] are shown at half-integer (a) and integer (b) values of Φ/Φ_0. The resistance has been measured using an ac current of 100 nA. At $\Phi = (n+1/2)\Phi_0$ pronounced resistance maxima appear for $n \geqslant 3$. The maximum value of the resistance R_{max} strongly increases with n and can become as high as 1.5 R_N for $n = 6$. In contrast, when $\Phi = n\Phi_0$ no anomalies are seen for $n \leqslant 4$. At the highest values of Φ/Φ_0, i.e., $\Phi = 5\Phi_0$ and $\Phi = 6\Phi_0$, relatively weak anomalies appear. On the other hand, the lead segment (voltage contacts V_1/V_3) next to the loop does not reveal any anomalies in the investigated field range. This is confirmed by the data shown in Fig. 14. From our physical picture we expect that the anomalies caused by the weak spot disappear when the whole structure becomes normal conducting. Indeed, the excess resistance for the loop segment always goes to zero when the temperature approaches the $T_c(B)$ of the lead segments (compare Figs. 13 and 14). The latter observation is in line with the disappearance of the anomalies in the samples of type A when approaching the phase boundary of the wire (see Figs. 9 and 10).

The results presented above clearly indicate a direct correlation between the height of the resistance maximum R_{max} and the local depression of the transition temperature for the loop segment. This correlation is further illustrated in Fig. 15 where the top panel shows the normalized height of the resistance peak $R_{max}/R_N - 1$ vs Φ/Φ_0 and the bottom panel shows the variation of ΔT_c vs Φ/Φ_0. From the data shown in Fig. 15 we can conclude that the periodic variations of ΔT_c induce proportional periodic variations of R_{max}/R_N. When comparing the top and bottom panels in Fig. 15 it appears that a certain critical value of $\Delta T_c \simeq 5$ mK has to be exceeded to obtain an anomalous resistance maximum near T_c. Our results also indicate that ΔT_c is small but nonzero for $\Phi = n\Phi_0$ with $n = 2,3,4,5$. This increase of ΔT_c with n is reflected by the appearance of a (smaller) resistance maximum for $\Phi = 5\Phi_0$ and $\Phi = 6\Phi_0$ [see Fig. 13(b)].

At this point we should note that the magnitude of the difference in $T_c(B)$ for the loop and the lead segment slightly fluctuates from sample to sample. A small astigmatism of the electron beam during the lithographic patterning may, e.g., account for the latter effect.[43] Some caution is also necessary when assigning T_c to the midpoint of the resistive transition. The resistively determined T_c could slightly differ from the mean-field transition temperature since the $R(T)$

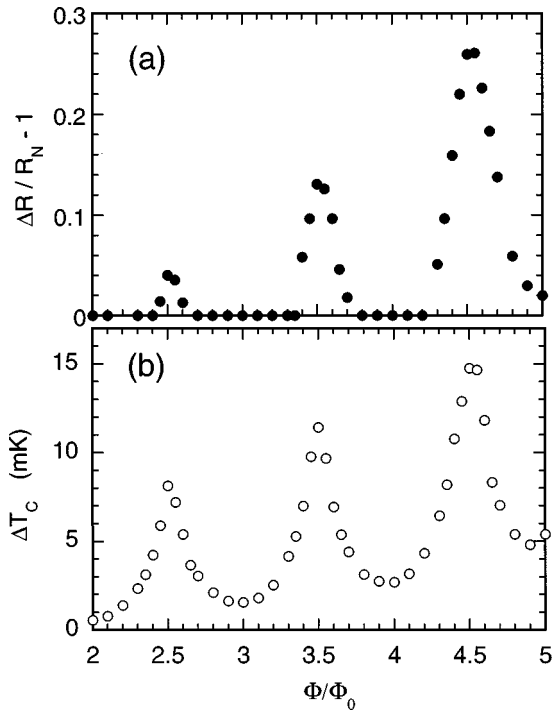

FIG. 15. (a) Normalized height $R_{\max}/R_N-1$ of the resistance anomaly and (b) difference in the critical temperature $\Delta T_c = T_c^{(\mathrm{lead})} - T_c^{(\mathrm{loop})}$ vs Φ/Φ_0 for sample B1.

curves are modified by nonequilibrium processes which are presumably responsible for the resistance maximum. Nevertheless, the $T_c(B)$ curves (see Fig. 12) for the loop extracted from the anomalous resistive transition at $\Phi \geqslant 2.5\Phi_0$ are in better agreement with the theoretical expectations than the $T_c(B)$ extracted from the resistance curves at $\Phi = 0.5\Phi_0$ and $\Phi = 1.5\Phi_0$ [see Fig. 13 (a)], which do not show a resistance maximum. We believe that the midpoint of $R(T)$ provides a reasonable indication for the mean-field transition temperature.

VII. DISCUSSION

A. Pro and contra of the charge imbalance scenario

Can the experimental observations described above be satisfactorily explained in terms of charge imbalance as described in Sec. II? In the following we discuss a number of arguments in favor and against that mechanism:

(1) Observations in favor of a charge imbalance effect:

(i) The charge imbalance near PSC's or N/S interfaces allows a qualitative understanding of the observed excess voltages (see Fig. 1).

(ii) The anomalies disappear when increasing the distance between the voltage probes (see Fig. 8).

(iii) The destruction of the negative spikes in dV/dI by a weak magnetic field agrees very well with the expected decrease of τ_{Q*} with increasing magnetic field (compare Figs. 10 and 11).

(iv) The nonlocal effect reported by Park *et al.*[8] In this paper a series of negative peaks in the dV/dI traces of one line segment is ascribed to the successive nucleation of PSC's in the *adjacent* line segments.

(v) The nucleation of PSC's at the weakest spots of the sample offers a simple understanding of why the anomalies always occur at specific spots in the sample.

(2) Observations in disagreement with a charge imbalance effect:

(i) Equation (3) grossly overestimates the amplitude of the resistance anomalies: using the parameters of Table I and $T_{c0}-T \simeq 15$ mK, one obtains from Eq. (4) $\Lambda_{Q*} \simeq 10\ \mu$m, which should result in an apparent resistance of $R \simeq 10 \times R_N$ for a 1 μm segment of sample A1. In contrast, the highest observed experimental value is $R \simeq 1.3 \times R_N$.

(ii) The disappearance of the anomalies in dV/dI when approaching T_{c0} (see Fig. 9) or $B_c(T)$ (see Fig. 10). Since τ_{Q*} diverges at the phase boundary, an increase rather than the observed decrease of the anomalies is expected.

(iii) The absence of discontinuities and hysteresis in $V(I)$ in the temperature range under consideration (within 50 mK below T_{c0}). Discontinuous changes of $V(I)$ are typical for the current enforced nucleation of PSC's.

B. Thermal activation vs current enforced nucleation of the PSC's

Looking back to the analysis of the experiments in the 1970s and early 1980s, the model of statistical thermal activation of the phase slip according to Langer and Ambegaokar[20] and McCumber and Halperin[21] (LA-MH) and the model of current enforced and discontinuous nucleation of PSC's according to Skocpol, Beasley, and Tinkham[25] (SBT) worked in different temperature regimes. The temperature range where the thermal activation of PSC's was important was restricted to a very narrow interval near T_c with a width of about 1 mK, while the current enforced nucleation of PSC's dominated within about 10 mK below T_{c0}. Consequently, the thermal activation effect was best observed in high-purity samples, i.e., whiskers, where the resistive transition was not additionally broadened by sample inhomogeneities which typically occur in thin films. The parameter controlling the width of the relevant temperature interval is the height of the energy barrier for the phase-slip, which is proportional to the sample cross section. Progress in sample fabrication in the late 1980s has resulted in a reduction of the cross section by two orders of magnitude, leading to a corresponding extension of the temperature interval where the thermal activation of the phase slip is important.[44] Thus, when approaching the critical temperature, it becomes more and more probable that the phase slip is triggered by thermal fluctuations for $I < I_c(T)$, implying that there must exist a crossover between the SBT and the LA-MH regimes. Such a crossover could possibly resolve difficulty 2(iii) (see Sec. VII A).

A possible synthesis of the two models has recently been proposed by Arutyunov.[9] The keypoint of his paper is based on the intuitive argument that the time average of the voltage drop across a PSC should be proportional to the frequency of the phase-slip events Γ_T and the decay time τ_{Q*} of the voltage pulses corresponding to individual phase slips. Accordingly, Arutyunov introduces a prefactor $\Gamma_T \tau_{Q*}$ to describe the time-averaged spatial variation of μ_p and μ_q [see Eq. (15) in Ref. 9], where Γ_T is calculated within the LA-MH theory, while the spatial dependence of μ_p and μ_q is taken

from the SBT model [see Fig. 1 and Eq. (2)]. The introduction of the prefactor $\tau_{Q*}\Gamma_T$ is incompatible with the assumption that the time average of the voltage across the PSC is linked to the phase-slip rate via the Josephson relation. The latter assumption has been used, however, throughout the previous literature on phase-slip centers, including the LA-MH and SBT models [see, e.g., Ref. 25, Eq. (4)]. Therefore, it appears that a microscopic theory consistently combining the thermal activation of the phase slip and the charge imbalance effects is still lacking.

In the already mentioned experiment by Park *et al.*,[8] two-dimensional samples with an artificially created normal/superconducting interface have been studied. Park *et al.* found anomalies in $R(T)$ and $V(I)$ which are very similar to ours and also rely on an explanation in terms of charge imbalance around PSC's. Intuitively, it appears unlikely that PSC's can nucleate in films much wider than the superconducting coherence length. Recently, however, experimental evidence was found that the onset of resistive behavior in wide superconducting strips occurs due to so-called phase-slip lines, which behave very similar to phase-slip centers in one-dimensional superconductors.[45] Park *et al.* also observe that the anomaly in $V(I)$ disappears close to T_{c0} but they do not provide data on the magnetic-field dependence.

C. Line structures vs loop structures

At first sight, there appears to be a difference in behavior between lines (structure A) and loops (structure B). In our experiments on line structures a certain dc or rf current load is necessary to activate the weak spot of the sample and generate the anomalies. The anomalies in loop structures appear without exceeding a critical current load, i.e., the resistance curves are insensitive to a small ac probe current $\lesssim 100$ nA for our samples. An explanation for this difference could be that the role of the dc or rf current load in case of the loops is taken over by the shielding current around the loop that maintains fluxoid quantization for $\Phi \neq n\Phi_0$. The experiments of the Cornell group[8,12] also show that resistance anomalies are present at negligible probe current load, when there is a substantial local reduction of T_c induced by the reactive ion etch.

Hence, it appears that the presence of resistance anomalies in the limit of vanishing current load requires a critical value for the suppression of T_c in the weak spot. As illustrated in Fig. 15, an increase of ΔT_c above 5 mK leads to the emergence of the resistance anomalies in the loop. This observation offers another — at least partial — solution of difficulty 2(ii) (see Sec. VII A), which is indicated by the suppression of the Little-Parks effect close to T_{c0} (see Fig. 12) and the simultaneous vanishing of the resistance anomalies for $\Phi=(n+1/2)\Phi_0$ [see the $R(T)$ curves for $n=0$, 1 and 2 in Fig. 13(a)]. As $\xi(T)$ diverges close to T_{c0}, the efficiency of the loop as the weak spot is strongly reduced. A similar effect is also expected for the weak spot in the line samples, which is consistent with the strong reduction of the negative dV/dI peaks in the 1.367 K trace of Fig. 9. The 1.373 K trace of Fig. 9 is already in the fluctuation regime above T_{c0}, confirming that the anomaly indeed vanishes in the normal state.

Very recently, Zhang and Price have measured the magnetic susceptibility of a single isolated Al loop as a function of temperature and magnetic flux.[46] They found that the phase-slip activation rate determined from histograms of individual phase-slip events is in reasonable agreement with a variant of the LA-MH theory for loops. Their results provide a direct test of the LA-MH theory for *equilibrium* phase fluctuations, which does not rely on transport measurements. Thus, the LA-MH theory may serve as a possible starting point for the inclusion of *nonequilibrium* effects such as charge imbalance, which appear to be important for the understanding of the transport experiments in mesoscopic wires.

D. Possible mechanisms for the rf generation of the anomalies

Finally, we briefly speculate about the possible causes of generation of the anomalies by rf irradiation. We have already discussed the effect of classical mixing, which can account for the resistance maximum but not for the excess voltages in $V(I)$. Another simple possibility is that the rf current exceeds the critical current of the weakest spot during a certain fraction of the rf cycle. Two things may happen: (i) the heat dissipated in the weak spot when it is in the normal state may be sufficient to keep it normal during the whole rf cycle, leading to a kind of SNS structure with an associated charge imbalance; (ii) the rf current triggers the phase-slip cycle as long as $I_{\rm rf}(t)>I_c(T)$ with a high enough rate to provide an average dc voltage which exceeds $R_N I_{\rm dc}$. Case (i) should be obtained when the frequency $\nu_{\rm rf}$ of the rf signal is comparable to or higher than the inverse energy relaxation time ($\tau_E \simeq 4$ ns). Besides the mixing effect discussed above, case (ii) could contribute to the anomalies observed at interference frequencies in the kHz range where $\nu_{\rm rf} \ll 1/\tau_E$. Note that in the frequency interval investigated in this work $\hbar\omega \ll \Delta(T)$, implying that there is no direct pair breaking by the rf current. In case of the $V(I)$ characteristics under rf irradiation [see Fig. 4(a) in Ref. 7] there is also no synchronization of the rf current and the phase-slip process, since the frequency of the rf current is fixed, while $V_{\rm dc}$ varies strongly close to the critical current.

To our knowledge, only a few theoretical calculations have addressed the influence of rf irradiation on the resistive state in superconducting filaments. Ivlev[47] has discussed the nucleation of a spatially inhomogeneous superconducting state induced by a rf electromagnetic field of frequency $\hbar\omega \ll \Delta(T)$. Churilov *et al.*[48] have reported electromagnetic oscillations in narrow superconducting wires containing PSC's with a frequency much lower than the Josephson frequency corresponding to the voltage across the PSC's. Gogadze[49] has interpreted the latter experiments in terms of multiple Andreev reflection of quasiparticles between the two N/S boundaries of the PSC. The external rf field may synchronize with these comparatively low-frequency oscillations.

VIII. CONCLUSIONS

We have studied resistance anomalies and excess voltages in one-dimensional mesoscopic superconductors. Great care has been taken to distinguish between intrinsic effects and spurious effects due to parasitic ac currents through the sample. The anomalies are absent very close to the magnetic

phase boundary $T_c(B)$ and appear when T_c is reduced by external perturbations like a rf field or a sufficiently high dc current. An interpretation in terms of charge imbalance around spots of locally reduced T_c has been discussed, which allows a qualitative understanding of the observed effects. A control experiment has been performed, in which a tunable local reduction of T_c has been achieved by using the Little-Parks effect of a loop integrated into the samples. Although many of the experimental findings fit into the scenario of nonequilibrium superconductivity, more theoretical work is required to provide a quantitative understanding of the behavior of the anomalous effects as a function of the various parameters like temperature, current, and magnetic field.

ACKNOWLEDGMENTS

We thank F. W. H. Hekking and K. Arutyunov for helpful discussions and M. Van Bael for providing the AFM pictures of the samples. The work at the K. U. Leuven has been supported by the Fund for Scientific Research - Flanders (FWO), as well as by the Flemish Concerted Action (GOA) and the Belgian Inter-University Attraction Poles (IUAP) research programs. The work at Northwestern University has been supported by the National Science Foundation under Grant No. DMR-9357506, and by the David and Lucile Packard Foundation. Travel between Leuven and Evanston was made possible through a NATO Collaborative Research Grant.

*Present address: Institut für Physik, Universität Basel, Klingelbergstr. 82, CH-4056 Basel, Switzerland. Electronic address: strunk@ubaclu.unibas.ch

[1] *Proceedings of the NATO Advanced Research Workshop on Mesoscopic Superconductivity*, edited by F. W. J. Hekking, G. Schön, and D. A. Averin, Karlsruhe, 1994 [Physica B **203**, 201 (1994)].

[2] P. Santhanam *et al.*, Phys. Rev. Lett. **66**, 2254 (1991).

[3] H. Vloeberghs *et al.*, Phys. Rev. Lett. **69**, 1268 (1992).

[4] J. J. Kim *et al.*, J. Phys.: Condens. Matter **6**, 7055 (1994).

[5] K. Yu. Arutyunov, *et al.* Czech. J. Phys. **46** Suppl. 2, 2311 (1996).

[6] I. N. Zhilyaev, I. N. Sosnin, P. Tuset, and K. Fossheim, Phys. Rev. B **54**, R9658 (1996).

[7] C. Strunk *et al.*, Phys. Rev. B **53**, 11 332 (1996).

[8] M. Park, M. S. Isaacson, and J. M. Parpia, Phys. Rev. Lett. **75**, 3740 (1995); Phys. Rev. B **55**, 9067 (1997).

[9] K. Yu. Arutyunov, Phys. Rev. B **53**, 12 304 (1996).

[10] B. Burk *et al.*, Superlattices Microstruct. **20**, 575 (1996).

[11] E. Spahn and K. Keck, Solid State Commun. **78**, 69 (1991).

[12] Y. K. Kwong *et al.*, Phys. Rev. B **44**, 462 (1991).

[13] S. Rubin *et al.*, Ann. Phys. (Leipzig) **1**, 492 (1992).

[14] A. Nordstrom and Ö. Rapp, Phys. Rev. B **45**, 12 577 (1992).

[15] A. W. Kleinsasser and A. Kastalsky, Phys. Rev. B **47**, 8361 (1993).

[16] R. Vaglio, C. Attanasio, L. Maritato, and A. Ruosi, Phys. Rev. B **47**, 15 302 (1993).

[17] W. A. Little and R. D. Parks, Phys. Rev. Lett. **9**, 9 (1962).

[18] R. P. Groff and R. D. Parks, Phys. Rev. **176**, 567 (1968).

[19] M. Tinkham, *Introduction to Superconductivity*, 2nd ed. (McGraw-Hill, New York, 1996).

[20] J. S. Langer and V. Ambegaokar, Phys. Rev. **164**, 498 (1967).

[21] D. E. McCumber and B. I. Halperin, Phys. Rev. B **1**, 1054 (1970).

[22] R. S. Newbower, M. R. Beasley, and M. Tinkham, Phys. Rev. B **5**, 864 (1972).

[23] W. W. Webb and R. J. Warburton, Phys. Rev. Lett. **20**, 461 (1968).

[24] J. Meyer and G. v. Minnigerode, Phys. Lett. **38A**, 529 (1972).

[25] W. J. Skocpol, M. R. Beasley, and M. Tinkham, J. Low Temp. Phys. **16**, 145 (1974).

[26] A. M. Kadin, L. N. Smith, and W. Skocpol, J. Low Temp. Phys. **38**, 497 (1980).

[27] B. I. Ivlev and N. B. Kopnin, J. Low Temp. Phys. **44**, 453 (1981).

[28] B. I. Ivlev and N. B. Kopnin, Adv. Phys. **33**, 47 (1984).

[29] A. Baratoff, Phys. Rev. Lett. **48**, 434 (1982).

[30] O. Liengme, A. Baratoff, and P. Martinoli, J. Low Temp. Phys. **65**, 113 (1986).

[31] G. J. Dolan and L. D. Jackel, Phys. Rev. Lett. **39**, 1628 (1977).

[32] M. Stuivinga, C. L. G. Ham, T. M. Klapwijk, and J. E. Mooij, J. Low Temp. Phys. **53**, 633 (1983).

[33] A. Schmid and G. Schön, J. Low Temp. Phys. **20**, 207 (1975).

[34] J. E. Mooij and T. M. Klapwijk, in *Localization, Interaction and Transport Phenomena*, edited by B. Kramer, G. Bergmann, and Y. Bruynseraede (Springer-Verlag, Berlin, 1985).

[35] C. C. Chi and J. Clarke, Phys. Rev. B **19**, 4495 (1979).

[36] A. M. Kadin, W. J. Skocpol, and M. Tinkham, J. Low Temp. Phys. **33**, 481 (1978). Although Eq. (6) was originally derived for the magnetic field parallel to the film plane, it is also valid for narrow wires in perpendicular field, provided that no vortices can nucleate in the wires [$d \lesssim \xi(T)$].

[37] M. Stuivinga, J. E. Mooij, and T. M. Klapwijk, J. Low Temp. Phys. **46**, 555 (1982).

[38] V. V. Moshchalkov *et al.*, Nature (London) **361**, 617 (1993).

[39] V. M. Dmitriev and E. V. Khristenko, JETP Lett. **29**, 697 (1979).

[40] The observation that the anomaly grows when the measuring current is increased appears to be in contradiction to the current dependence of the data reported in Ref. 3. In this early experiment the electrical leads were not filtered, the anomaly was observed at low ac measuring currents and it was suppressed for higher amplitudes of the ac current. While the presence of the anomaly at low currents was most probably due to rf interference, its apparent destruction by a high ac current is a simple consequence of the strong nonlinearity of $V(I)$ at I_c. Since $V(I)$ is essentially zero in the time intervals where $I(t) = I_{ac} \cos(\omega t) < I_c(T)$, the Fourier component V_ω corresponding to the measuring frequency (which is detected by the lock-in technique) is reduced. This leads to a strong rounding of the upper part of the resistive transition and suppresses the resistance enhancement $R > R_N$. The normal-state resistance is recovered only for $I_{ac} \gg I_c(T)$.

[41] W. J. Skocpol and L. D. Jackel, Physica B & C **108**, 1021 (1981).

[42] C. Strunk *et al.*, Phys. Rev. B **54**, R12 701 (1996).

[43] Such an astigmatism can cause a difference in the average linewidth d of the leads and the square loop. Since $\Delta T_c \propto d^2$ [see Eq. (7)] a difference in mean linewidth of 5% could account for the observed $\Delta T_c \simeq 5$ mK at $\Phi = 5\Phi_0$.

[44] N. Giordano, Phys. Rev. Lett. **61**, 2137 (1988).

[45] A. P. Zhuravel, A. G. Sivakov, O. G. Turutanov, and I. M. Dmitrenko, Czech. J. Phys. **46** Suppl. S-2, 643 (1996); see, also, I.

M. Dmitrenko, Sov. J. Low Temp. Phys. **22**, 648 (1996), and the references therein.
[46] X. Zhang and J. C. Price, Phys. Rev. B **55**, 3128 (1997).
[47] B. I. Ivlev, Sov. Phys. JETP **45**, 626 (1977).
[48] See, e.g., G. E. Churilov, D. A. Dikin, V. M. Dmitriev, and V. N. Svetlov, Sov. J. Low Temp. Phys. **17**, 96 (1991), and references therein.
[49] G. A. Gogadze, Sov. J. Low Temp. Phys. **12**, 622 (1986).
[50] J. Romijn, T. M. Klapwijk, M. J. Renne, and J. E. Mooij, Phys. Rev. B **26**, 3648 (1982).